Effects of evanescent waves in phononic crystals with linear defects

V. Romero-Garcia, Ruben Pico, Jerome O. Vasseur, Anne-Christine Hladky, Victor Sanchez-Morcillo, Lluis Miquel Garcia-Raffi

Effects of evanescent waves in phononic crystals with linear defects

V. Romero-Garcia[a], R. Pico[a], J. Vasseur[b], A.-C. Hladky-Hennion[b], V. Sanchez-Morcillo[a] and L.M. Garcia-Raffi[a]

[a]Universidad Politecnica de Valencia, Paranimf 1, 46730 Gandia, Valencia, Spain, 46730 Gandia, Spain

[b]IEMN département ISEN, UMR CNRS 8520, 41 boulevard Vauban, 59046 Lille Cedex, France

virogar1@gmail.com

Periodic structures with linear defects have been traditionally analyzed with the $\omega(\vec{k})$ methods with the supercell approximation. The presence of the linear defect introduces guided modes at frequencies in the band gap of the complete structure. This methodology only considers the propagating properties of the periodic system. In this work we report both theoretical predictions and experimental results considering both the evanescent and propagating waves. We obtain the evanescent properties from the complex band structures solving the inverse problem $k(\omega)$ with the Extended Plane Wave Expansion (EPWE). From the Fourier transform of the complex eigenvectors we obtain the acoustic field profile inside the system showing both the evanescent and the propagating properties. A good agreement between both the Multiple Scattering predictions and data with the EPWE simulations is obtained. The presence of evanescent waves is of fundamental interest for the design of devices based on periodicity providing a complete picture of the physical properties of the system.

1 Introduction

The control of evanescent waves in periodic systems has been revealed of fundamental interest in last years. On one hand, fundamental questions related to the band gap (BG) properties of periodic structures have been theoretically [1, 2, 3] and experimentally [4] reported. In this sense, the complex band structures, which are the dispersion relation taking into account both the propagating and evanescent modes, reveal the BGs as ranges of frequencies where only evanescent modes can be excited in the system. A particular kind of bands in periodic systems are known as deaf bands [5, 6]. The analysis of the evanescent properties of the periodic systems has shown the correct interpretation of these deaf bands as ranges of frequencies where evanescent waves with the correct symmetry are excited in the system [7]. Periodic structures with point defects have been also analyzed in terms of evanescent waves, accurately characterizing the evanescent coupling between the localized modes [8]. On the other hand, more applied phenomena related with evanescent waves has been observed [9, 10]. In these works the control of evanescent properties enables the imaging with super resolution, i.e., overcoming the diffraction limit. This can be obtained by restoring all the evanescent components of a near-field image. The mechanism used in these works was based on the coupling of the evanescent modes with other mechanism leading to their amplification in order to successfully transport the information carried by the evanescent waves through the system. Recently, the possibility to control the evanescent properties in periodic composites has shown several interesting possibilities in both photonic [11, 12] and phononic [13, 14, 15] crystals. In this way, the evanescent properties of the periodic systems have been revealed necessary for the design of new acoustic and electromagnetic applications.

The extended plane wave expansion (EPWE) with supercell approximation [8] represents one of the possibilities to evaluate the excited evanescent modes in periodic structures with defects. This methodology is more general than the classical ones, $\omega(\vec{k})$, revealing a complete picture of the physics of the systems. Recent works [16, 17] show the accurate results obtained in two dimensional (2D) sonic crystal waveguides (SCW), revealing novel properties never observed in the classical methods. The SCW is created by removing one row scatterers of the periodic structure. In this work we review the theoretical and experimental results of in SCW, showing the experimental setup, the Multiple Scattering results and the comparison with the EPWE.

Using the classical $\omega(\vec{k})$ methods one can find two kinds of bands, the propagating and the deaf ones [5] and no information can be obtained about the evanescent modes. We show here that the complex band structure reveals additional bands related with evanescent modes, never predicted by the $\omega(\vec{k})$ methods, that drastically change the propagation properties of the system. Figure 2a shows the complex band structure for a SCW in the ΓX direction (through the work reduced magnitudes have been used, $\Psi = \nu a/c_{host}$, $K = ka/(2\pi)$). Left and right (respectively, middle) panels represent the imaginary (respectively, real) part of the complex band structures. The classification shown in this work, inspired by the works of Bavencoffe [21] helps to a better understanding of the complex band structures. The convergence of all the calculations has been carefully analyzed selecting the adequate number of plane waves for each case. The modes are classified following the next restrictions: (*i*) The classical band structures correspond to modes characterized by values of $Re(K)$ in the Brillouin zone and $Im(K) = 0$. Modes with these properties are shown in this work with black filled circles. (*ii*) The modes characterized by $Im(K) \geq 0$ and $Re(K) = 0$ are shown with red filled triangles. These modes represent connections between propagating bands at the Γ point. (*iii*) The modes characterized by $Im(K) \geq 0$ and $Re(K) = 1/2$ (respectively, $Re(K) = 1/\sqrt{2}$) are shown with green filled squares. These modes represents connections between propagating bands at the X (respectively, M) point. (*iv*) The modes with $Re(K)$ in the first Brillouin zone but with $Im(K) \neq 0$ are in this Section in blue filled diamonds. These modes belong to evanescent connecting bands between bands with the same symmetry crossing the Brillouin zone.

2 Experimental setup

The experiments showed in this work have been performed in an echo-free chamber sized $8 \times 6 \times 3$ m^3. To obtain the experimental dependence of the pressure all along the SCW, we measured the pressure field inside the guide. We build a finite SC hunging the rigid scatterers on a periodic frame (Figure 1) and the SCW is generated removing the central row of the complete structure. We notice that this system avoids the excess attenuation effect [19]. The finite 2D SC is made of 7×7 rigid cylinders arranged as a square array of lattice constant a. The radius of the cylinders used in the experiments is $r = 9$ cm, and the lattice constant of the SC is $a = 19$ cm. With these parameters, the filling fraction of the finite SC is $ff = \frac{\pi r^2}{a^2} \simeq 0.71$. The dimensions of the system are large enough for the microphone to be placed inside the waveguide. The microphone used is a prepolarized free-field 1/2" Type 4189 B&K. The diameter of the microphone is 1.32 cm, which is approximately $0.07a$, therefore a low level of influence over the pressure field measured is expected. The

source is placed 1 m away from the SCW launching white noise.

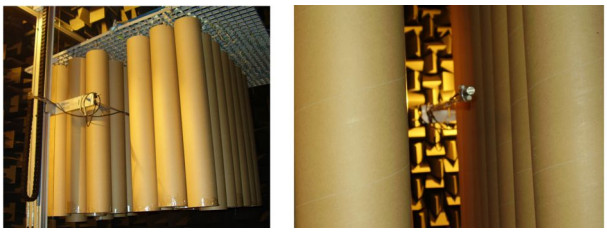

Figure 1: Experimental setup.

3 Evanescent waves in Sonic Crystal Waveguides

This Section shows the analysis of the complex band structures of SCW using the EPWE method. First of all we pay attention to the bands excited in the range of frequencies of the BG of the perfect SC (Figure 2a). Among the classical propagating and deaf bands [20], we can observe evanescent connections (blue diamonds and green square lines). To analyze their properties, we analyze three different modes marked in the Figure with red squares. The mode 1 ($\Psi_1 = 0.484$, $K_1 = 1/2 + 0.049\imath$) belongs to a connecting evanescent band (green squared line) between two symmetric propagating bands. Notice that at the same frequency in the real part there is a deaf band (antisymmetric) that does not contribute to the propagation properties. The absolute value of the acoustic field obtained from the Fourier transform of the eigenvectors, shown in Figure 2d1 is in agreement with the predictions of the scattering problem shown in Figure 2b which are also experimentally measured using our experimental set up (Figure 2e). One can also observe the decay rate of the mode as it penetrates in the waveguide. This decay is related with the imaginary part of the Bloch vector predicted by EPWE, $Im(K_1) = 0.049$. Fitting this decay to an exponential, ae^{-bx} [4, 3], we obtain $b = 0.053 \pm 0.004$ with fairly good agreement with EPWE. On the other hand, the mode 2 ($\Psi_2 = 0.619$, $K_2 = 0.346$) belongs to a guiding (symmetric) band. Notice that for this frequency, the evanescent connection (green squared line) appears between two antisymmetric (deaf) bands therefore the evanescent mode cannot be excited. The MST predictions for this propagating mode is shown in Figure 2c and the experimental evidence is shown in Figure 2f.

We would like to pay special attention to mode 3 ($\Psi_3 = 0.731$, $K_3 = 0.3 + 0.21\imath$) in Figure 2a. This mode belongs to a complex band with real part inside the first Brillouin zone (blue diamond line). Notice that this evanescent symmetric band connects two symmetric (guided) bands. The maximum value of the lower band appears in the Γ point (open black circle) whereas the minimum value of the upper band appears at the X point (open black circle), as a consequence the real part of the evanescent connection crosses the Brillouin zone. This kind of bands is not observed by the classical $\omega(\vec{k})$ methods and it could considerably contribute to the propagation properties as we will see later. The acoustic field predicted by the Fourier transform of the eigenvectors again coincides with the predicted field using MST shown in Figure 2d. Notice the good agreement between the theoretical prediction and the experimental results in Figure 2g. On the other hand, for this case EPWE predicts a decay rate equal to $Im(K_3) = 0.21$ which coincides with the fit from the MST prediction, $b = 0.21 \pm 0.03$.

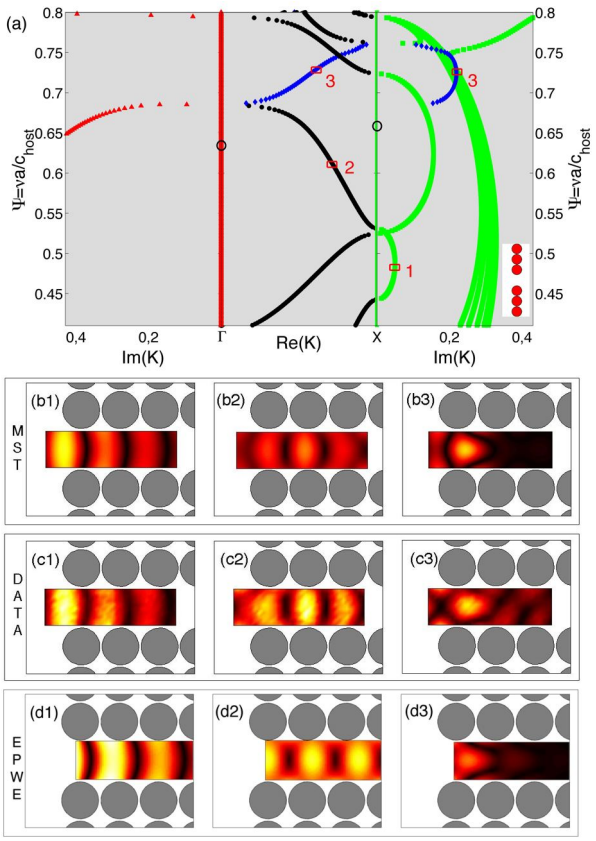

Figure 2: Theoretical and experimental analysis of the SCW. (a) Complex band structures for the SCW. 1681 plane waves have been used in the calculation. The supercell used in the calculations is shown in the inset. Reduced magnitudes have been plotted. (b1-b3) Absolute value of the acoustic field predicted using MST for frequencies (left panel) $\Psi_1 = 0.484$, (middle panel) $\Psi_2 = 0.619$ and (right panel) $\Psi_3 = 0.731$. (red squares in (a)). (c1-c3) show the experimental results of the absolute value of the acoustic field for frequencies Ψ_1, Ψ_2 and Ψ_3. (d1-d3) show the experimental results of the absolute value of the acoustic field for frequencies Ψ_1, Ψ_2 and Ψ_3.

4 Evanescent waves in Sonic Crystal Stubbed Waveguides

The presence of the stub or a defect in a SCW alters drastically the transmission spectrum. Although the general characteristics of the transmission properties of the SCW are preserved once the stub or the defect is created in the waveguide, narrow attenuation peaks appear in the guided bands occurring at the resonance modes of the stub. The stub modes are evanescent and strongly localized by the surrounding periodic structure.

Stubs are generated in this work by removing a scatterer in the side-wall of the waveguide. In this Section, we investigate both theoretically and experimentally the occurrence of

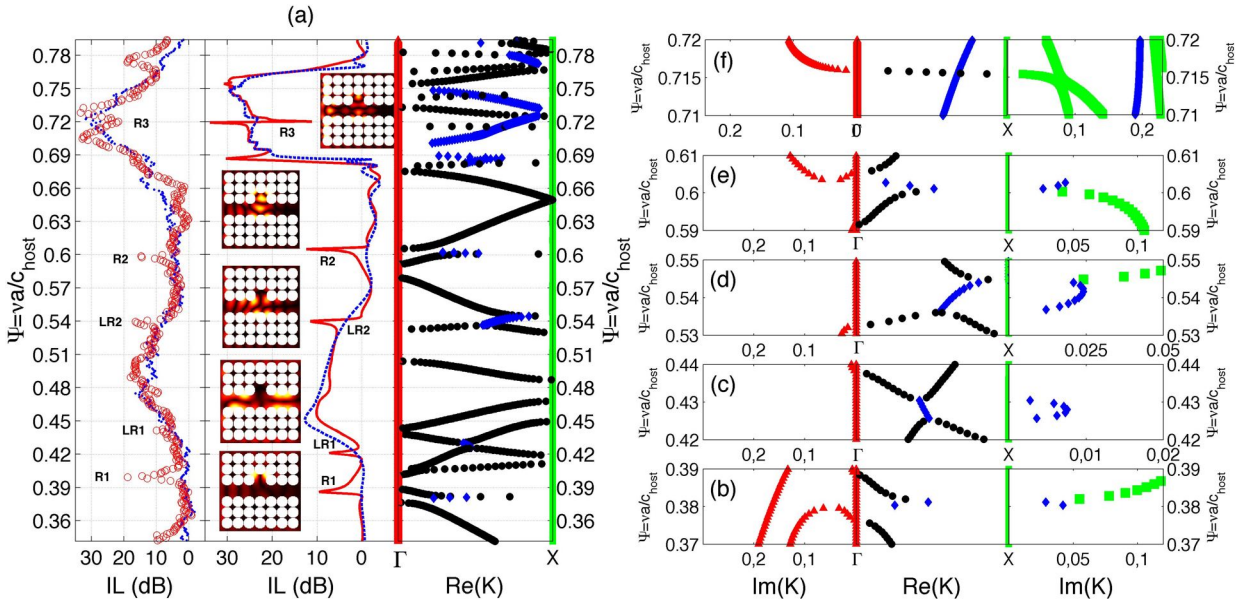

Figure 3: Theoretical and experimental analysis of the stubbed waveguide using EPWE and MST. (a) IL spectrum evaluated at the end of the waveguide. In the central panel blue continuous line (red dashed line) represent the MST predictions and in the left panel blue dots (open red circles) represent the experimental results of the SCW (stubbed SCW). Peaks labelled as R (LR) represent the effect of the resonances of the stub (effect of the level repulsion between bands with different symmetry). The right panel represents the real part of the complex band structure for the SCW. (b)-(f) show the details of both the hybridization of the resonances and the guide or evanescent modes and the repulsion between bands (see text).

the effects produced by a stub in a SCW. We observe two different effects due to the stub. On one hand, EPWE predicts attenuation dips due to the interaction of both the guided and the evanescent modes with the resonances of the stub. This result constitutes a proof of the importance of the $k(\omega)$ methods because they predict the evanescent bands and, as a consequence, the interaction between the evanescent modes and the resonances of the stub. The attenuation peaks in Figure 3a marked with R (resonance) correspond to this first effect and they will be discussed in detail Section **??**.

Chen *et al.* showed that depending on the symmetry of the system with respect to the incident direction of the incident wave, shear-horizontal modes either couple or not with the Lamb wave modes which are polarized in the sagittal plane. The coupling can be observed by a splitting between bands in the band structure and by a transfer of the symmetry from one band to the other. In the case in which no coupling occurs, the symmetric Lamb waves band simply crosses of the shear-horizontal band. Similar results have been recently observed in 1D phononic crystals [18, 21], and anisotropic phononic crystals [6]. Some similar results are shown in this work. We observe that the repelled bands are connected by an evanescent mode which is the responsible of the transfer of the symmetry from one band to another. The attenuation peaks in Figure 3a marked with LR (level repulsion) correspond to this second effect and they will be discussed in detail in Section **??**.

The real part of complex band structures of the stubbed waveguide are also shown in the right panel of the Figure 3a. One can observe the correspondence between the attenuation peaks, R and LR, predicted by MST (central panel of Figure 3a) and the singular points of the band structure. Left panel of Figure 3a shows the experimental data, in good agreement with the theoretical predictions. Let us study the nature of each of these attenuation peaks.

4.1 Resonances

The stub acts as a resonant cavity in the waveguide producing flat bands due to the localized mode in the stub. If this resonance occurs at the same frequency as a guiding or evanescent bands, then the hybridization of the two bands produces an attenuation peak in the spectrum. Resonances of the stub, calculated using EPWE at point X, can be observed in Figure **??**. It is worth noting that the frequencies of these resonances coincide with two symmetric guiding bands and one evanescent band of the waveguide.

Points R1 (Ψ = 0.3812) and R2 (Ψ = 0.605) in Figure 3a coincide with the hybridization of the guiding bands and the resonance bands of the stub (flat band). A detailed image of the hybridization effect at these frequencies can be seen in Figures 3b and 3e. These hybridizations explain the attenuation peaks in the IL spectrum labelled as R1 and R2 in Figure 3a in good agreement with both the analytical predictions and the experimental results. The slight disagreements between the experimental data and the theoretical predictions can be due to the sensitivity of the experimental data to the size of the stub.

Point R3 (Ψ =0.72) corresponds to the interaction of an evanescent mode with the resonance of the stub at this frequency. The detailed band structure for this frequency is shown in Figure 3f. Note that for this case no hybridization is produced and two bands can be excited. Once the wave penetrates in the SCW the evanescent mode is excited and, if the stub is as close as the evanescent mode can travel through the SCW, the stub mode should be excited. These results are not predicted by the classical methods, therefore they cannot be explained with the PWE, but EPWE gives the correct understanding of the phenomenon.

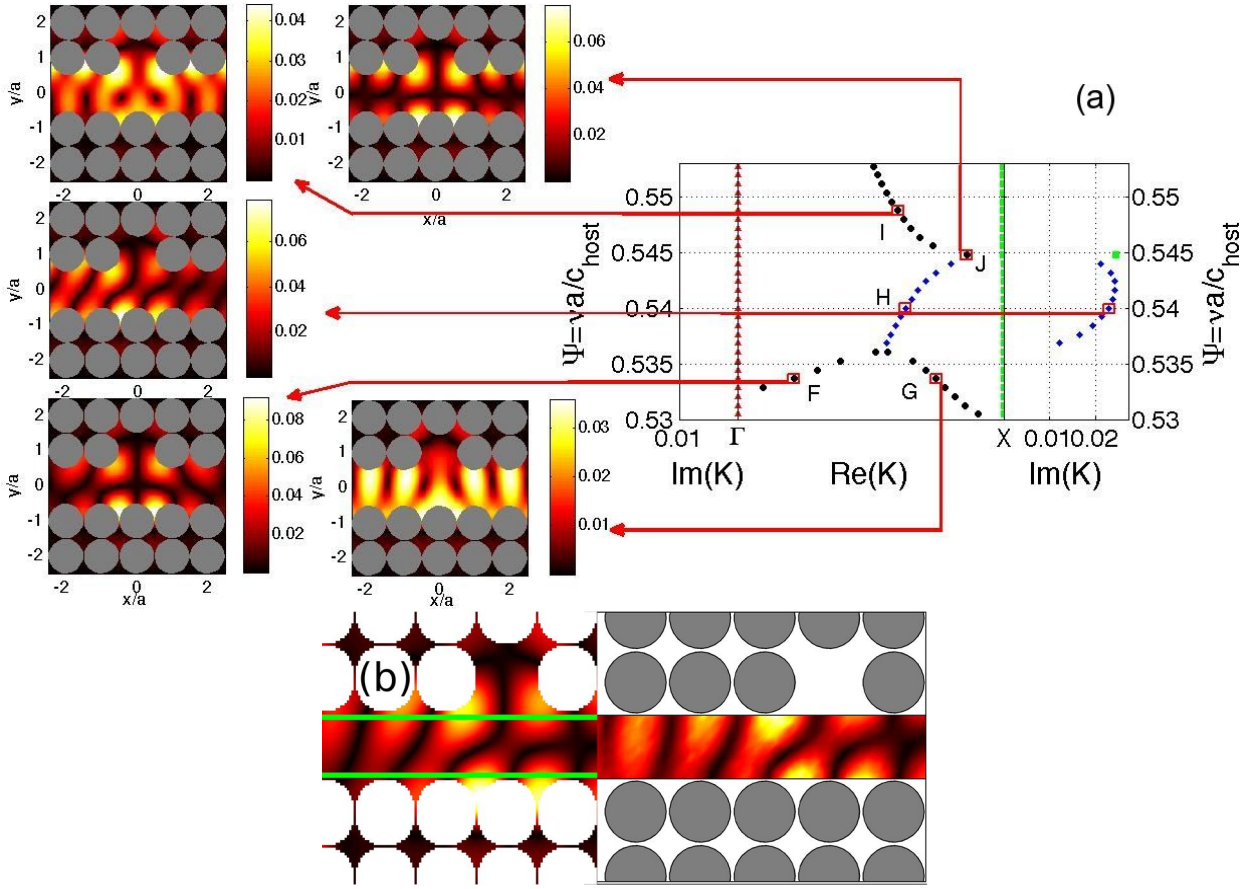

Figure 4: Analysis of the symmetry transfer between the repelled bands in stubbed waveguides. (a) The analysis corresponds to the repulsion state shown in Figure 3f and 3e respectively. The acoustic fields are represented using the absolute value of the pressure obtained from the Fourier transform of the eigenvectors for the eigenvalues marked with red squares. (b) Experimental results (right panel) and MST simulations (left panel) of the mode shown in (a) as H.

4.2 Level Repulsion States

Very recent works [6] have shown several kinds of crossing points in anisotropic phononic crystals. As a general rule for these systems, the bands involved in the crossing point, or level repulsion state, exchange their polarization, so that the polarization remains a continuous function of the wave vector $\vec{k}$. For the case of SC in which only longitudinal polarization is allowed, one can observe symmetric and antisymmetric acoustic fields. In our case, if the SCW is symmetric with respect to the incident acoustic field, only symmetric acoustic fields will be supported. However, if the system is non symmetric, then both symmetric and antisymmetric fields can be supported. The stubbed SCW is an example of a non symmetric system.

As a consequence of the presence of the stub in the SCW, the IL spectrum (Figure 3a) predicts two additional attenuation peaks referred to as LR1 (Ψ =0.429) and LR2 (Ψ =0.544). These peaks have different phenomenology than R1, R2 or R3 peaks which are due to the interaction between the guided or evanescent modes with the stub resonances (see previous Section). Oppositely, the LR1 and LR2 peaks correspond to crossing points in the band structure shown in Figure 3b. The presence of the stub changes the symmetry of the system, therefore antisymmetric modes can be excited even by symmetric longitudinal incident waves. This produces the appearance of repulsion states between symmetric and antisymmetric bands. In this work we observe that due to the local breaking of the symmetry because of the presence of the stub, a repelling state appears between symmetric and antisymmetric bands accompanied by a transfer of the symmetry of the modes from one band to the other.

In our case, the points LR1 and LR2 correspond to level repulsion states in the band structures that introduce a local band gap. The level repulsion state for these cases appears due to the crossing between an antisymmetric and a symmetric bands in a similar way as in phononic crystals thin plates [22, 18, 21]. Figures 3c and 3d represent detailed views of the band structures calculated using EPWE for the points LR1 and LR2 respectively. One can see that, in both cases, the repelled bands are connected by means of an additional band, which is evanescent. Thus, EPWE does not predict a repulsion level state but an evanescent connection between bands.

In order to analyze in more details the phenomenology involved in these level repulsion states, we have analyzed several modes for different frequencies all along the bands involved in the repulsion. Figure 4a shows the acoustic fields obtained from the Fourier transform of the eigenvectors for several modes in the repelled bands. The analyzed modes are marked with red squares which are connected using red arrows with their corresponding acoustic fields obtained usign EPWE.

One can observe that the modes in the repelled bands present a completely real eigenvalue whereas the connection bands have complex eigenvalue. The repelled bands are pre-

dicted by EPWE and they are exactly the same as the ones predicted by the PWE, however the difference appears in the evanescent connection between the repelled bands.

First, we fix our attention on the acoustic fields in the repelled bands. One can observe in Figure 4 that for each band, depending on the position with respect to the evanescent connection, different symmetries of the field can be excited. For example points F and G that belong to the same band have different symmetries. F is on the left of the evanescent connection and G is on the right of the evanescent connection. The acoustic field corresponding to the point G is mainly symmetric. However the acoustic field for the point F is completely antisymmetric. Then, inside the band (point H), there is an exchange of the symmetry, so that the symmetry remains a continuous function of the wave vector for each band. For the points I-J the situation is the same as in F-G.

The repelled bands are connected by an evanescent band which is the responsible of the exchange of symmetry between bands. The acoustic fields of the modes inside the evanescent connection have a mixed symmetry. We have studied the mode H in the evanescent connection. First of all one can see the mixed symmetry of the acoustic field of the mode. Moreover, one can observe the evanescent behaviour of the acoustic field inside the guide with a low decay rate indicating the small value of the imaginary part of the eigenvalue. Figure 4b shows the experimental data in comparison with the MST simulations. One can observe the good agreement between the two theoretical methods (EPWE and MST) and the experimental results.

5 Conclusions

The relevance of the evanescent modes in sonic crystals is theoretically and experimentally reported in this work. The complex bands structure, $k(\omega)$, calculated using the Extended Plane Wave Expansion reveals the presence of evanescent modes in these systems, never predicted by the traditional usual numerical $\omega(\vec{k})$ methods. The interpretation of the evanescent modes introduces novel explanations of the deaf bands as well as of the level repulsion states in antisymmetric periodic systems. In this work we observe that in the ranges of frequencies where a deaf band is traditionally predicted an evanescent mode with the excitable symmetry appears changing drastically the transmission properties. On the other hand, the simplicity of the sonic crystals in which only the longitudinal polarization can be excited, is used here to interpret, without loss of generality, the level repulsion between symmetric and antisymmetric bands in sonic crystals as the presence of an evanescent mode connecting both repelled bands. These evanescent modes explain both the attenuation produced in this range of frequencies and the transfer of symmetry from one band to the other. The experimental evidence of the level repulsion and the evanescent coupling are in very good agreement with the theoretical predictions.

Acknowledgments

This work was supported by MCI Secretaría de Estado de Investigación (Spanish government) and the FEDER funds, under grant MAT2009-09438, FIS2011-29734-C02-02, and from Generalitat Valencia through the project GV/2011/055. VRG is grateful for the support of "Programa de Contratos Post-Doctorales con Movilidad UPV (CEI-01-11)".

References

[1] R. Sainidou, N. Stefanou, I. Psarobas and A. Modinos. A layer-multiple-scattering method for phononic crystals and heterostructures of such. *Computer Physics Communications*, 166, 197, (2005)

[2] V. Laude, Y. Achaoui, S. Benchabane, and A. Khelif. Evanescent bloch waves and the complex band structure of phononic crystals. *Phys. Rev. B*, 80, 092301, 2009.

[3] V. Romero-García, J. V. Sánchez-Pérez, and L. M. Garcia-Raffi. Evanescent modes in sonic crystals, Complex dispersion relation and supercell approximation. *J. Appl. Phys.*, 108, 044907, 2010.

[4] V. Romero-García, J. V. Sánchez-Pérez, S. Castiñeira Ibáñez, and L. M. Garcia-Raffi. Evidences of evanescent bloch waves in phononic crystals. *Appl. Phys. Lett.*, 96, 124102, 2010.

[5] J. V. Sánchez-Pérez, D. Caballero, R. Martínez-Sala, C. Rubio, J. Sánchez-Dehesa, F. Meseguer, J. Llinares, and F. Gálvez. Sound attenuation by a two-dimensional array of rigid cylinders. *Phys. Rev. Lett.*, 80(24), 5325, 1998.

[6] Y. Achaoui, A. Khelif, S. Benchabane, and V. Laude. Polarization state and level repulsion in two-dimensional phononic crystals and waveguides in the presence of material anisotropy. *J. Phys. D, Appl. Phys.*, 43, 185401, 2010.

[7] V. Romero-García, L. M. Garcia-Raffi, and J. V. Sánchez-Pérez. Evanescent waves and deaf bands in sonic crystals *AIP Advances* 1, 041601 (2011)

[8] V. Romero-García, J. V. Sánchez-Pérez, and L. M. Garcia-Raffi. Propagating and evanescent properties of double-point defects in sonic crystals. *New. Jour. Phys.*, 12, 083024, 2010.

[9] J. B. Pendry. Negative Refraction Makes a Perfect Lens *Phys. Rev. Lett.* 85, 3966, 2000.

[10] N. Fang, H. Lee, C. Sun and X. Zhang. Sub-Diffraction-Limited Optical Imaging with a Silver Superlens *Science*, 308, 534, 2005.

[11] X. Li, S. He and Y.Jin Subwavelength focusing with a multilayered Fabry-Perot structure at optical frequencies *Phys. Rev. B*, 75, 045103, 2007.

[12] J. W. Dong, H. H. Zheng, Y. Lai, H. Wang and C. T. Chan Metamaterial slab as a lens, a cloak, or an intermediate *Phys. Rev. B* 83, 115124, 2011.

[13] A. Sukhovich, B. Merheb, K. Muralidharan, J. O. Vasseur, Y. Pennec, P. A. Deymier, and J. H. Page. Experimental and theoretical evidence for subwavelength imaging in phononic crystals. *Phys. Rev. Lett.*, 102, 154301, 2009.

[14] J. F. Robillard, J. Bucay, P. A. Deymier, A. Shelke, K. Muralidhraran, B. Merheb, J. O. Vasseur, A. Suckovich and J. H. Page. Resolution limit of a phononic crystal superlens *Phys. Rev. B* 83, 224301, 2011.

[15] J. Zhu, J. Christensen, J. Jung, L. Martin-Moreno, X. Yin, L. Fok, X. Zhang, and F. J. Garcia-Vidal. A holey-structured metamaterial for acoustic deep-subwavelenght imaging. *Nature physics*, 7, 52, 2011.

[16] V. Romero-García, J. O. Vasseur, A. C. Hladky-Hennion, L. M. Garcia-Raffi, and J. V. Sánchez-Pérez Level repulsion and evanescent waves in sonic crystals *Phys. Rev. B* 84, 212302 (2011)

[17] V Romero-García, J O Vasseur, L M Garcia-Raffi and A C Hladky-Hennion. Theoretical and experimental evidence of level repulsion states and evanescent modes in sonic crystal stubbed waveguides. *New J. Phys.* 14, 023049, (2012)

[18] M. Bavencoffe. PhD thesis, University of Le Havre, 2009.

[19] V. Romero-García, J. V. Sánchez-Pérez, and L. M. Garcia-Raffi. Analytical model to predict the effect of a finite impedance surface on the propagation properties of 2d sonic crystals. *J. Phys. D, Appl. Phys.*, 44, 265501, 2011.

[20] J. O. Vasseur, P. A. Deymier, M. Beaugeois, Y. Pennec, B. Djafari-Rouhani, and D. Prevost. Experimental observation of resonant filtering in a two-dimensional phononic crystal waveguide. *Z. Kristallogr*, 220, 829, 2005.

[21] M. Bavencoffe, B. Morvan, J. L. Izbicki, and A. C. Hladky-Hennion. Characterization of evanescent ultrsonic waves in a band gap of a 1d phononic crystal. *IEEE International Ultrasonics Symposium Proceedings*, page 1024, 2009.

[22] J. J. Chen, B. Bonello, and Z. L. Hou. Plate-mode waves in phononic crystal thin slabs, Mode conversion. *Phys. Rev. E*, 78, 036609, 2008.